Available online at www.sciencedirect.com
ScienceDirect
Journal of Power Sources 177 (2008) 470–477
JOURNAL OF POWER SOURCES
www.elsevier.com/locate/jpowsour

Preparation and characterization of Ir/TiC catalyst for oxygen evolution

Lirong Ma [a,b], Sheng Sui [b,*], Yuchun Zhai [a]

[a] School of Materials & Metallurgy, Northeastern University, Shenyang 110004, China
[b] Institute of Fuel Cell, Shanghai Jiao Tong University, Shanghai 200240, China

Received 25 November 2007; accepted 27 November 2007
Available online 15 January 2008

Abstract

Nano-sized titanium carbide (TiC) was employed as the support material for an iridium (Ir) electrocatalyst in a proton exchange membrane water electrolyser (PEMWE). The Ir/TiC electrocatalyst for the oxygen evolution reaction (OER) was prepared by chemical reduction and deposition with ultrasonic dispersion. The diameter of the Ir particles deposited on the TiC support is 10–40 nm. The Ir/TiC catalyst has a pore volume of 0.1425 $cm^3\ g^{-1}$, which is about two times as high as that of the corresponding unsupported Ir. Scanning electron microscopy (SEM), transmission electron microscopy (TEM), X-ray diffraction (XRD) and energy dispersive X-ray (EDX) analysis indicate that the Ir particles are nearly uniformly deposited on the surface of the TiC and exhibit remarkably fine variable crystallites and crystal lattice defects, which enhance the density of active sites and greatly improves the catalytic activity of the Ir/TiC catalyst. Cyclic voltammograms (CVs) reveal that the peak current density at 1.5 V versus SCE on the Ir/TiC is about nine times of that for the unsupported Ir black catalyst and potentiostatic analysis shows that the charge passed by the Ir/TiC after 600 s at 1.3 V versus SCE is about 15 times of that for the unsupported Ir catalyst. Electrochemical impedance spectroscopy (EIS) shows that the electrochemical polarization impedance of the Ir/TiC catalyst is about 50 $\Omega\ cm^2$ per 0.02 mg as compared to 150 $\Omega\ cm^2$ of the Ir black in the range of high frequency. The diffusion polarization impedances of the Ir/TiC form a semicircle and those of the Ir black are close to a straight line with a phase angle of 45° in the range of low frequency. Thus, the catalytic activity of the Ir/TiC for the OER is significantly higher than that of the unsupported Ir catalyst. The TiC support is chemically and electrochemically stable in the whole range of experimental potentials.

Keywords: Oxygen evolution; Support; Catalysts; Proton exchange membrane water electrolyser; Cyclic voltammogram; Electrochemical impedance spectroscopy

1. Introduction

Hydrogen as a clean and environmentally acceptable fuel is expected to be one of the most promising energy sources in the near future. The proton exchange membrane fuel cell (PEMFC), a power generation device with higher energy conversion efficiency and environmental compatibility using hydrogen and oxygen as the energy medium, is one of the attractive options for producing clean energy. However, the major hurdle for commercialization of the PEMFC is how to generate and supply pure hydrogen directly. The relatively simple methods to supply hydrogen include the water electrolyser (WE) and regenerative fuel cell (RFC). The RFC can be operated in both the fuel cell (FC) and WE modes [1]. The proton exchange membrane water electrolyser (PEMWE) and regenerative proton exchange membrane fuel cell (RPEMFC) based on proton exchange membrane as electrolytes are among the most promising methods for hydrogen generation.

The performances of the PEMWE and RPEMFC mainly depend on the electrochemical characteristics of the oxygen electrodes. Both of them include a WE unit, in which hydrogen and oxygen are generated by splitting water using electrical power. One of the key challenges limiting the commercialization of the PEMWE and RPEMFC is the catalyst activity for oxygen evolution. The oxygen evolution reaction (OER) is the main source of energy loss in electrochemical cells involving oxygen electrodes. It is believed that the overpotential at which the oxygen anode operates is influenced by absorbed species at the metal surface that block the approach of oxygen-containing species to the surface sites where they are going to be oxidized. The oxygen electrode catalysts must also be resistant to anodic corrosion during oxygen evolution because the

* Corresponding author. Tel.: +86 21 34206249; fax: +86 21 34206249.
E-mail address: ssui@sjtu.edu.cn (S. Sui).

0378-7753/$ – see front matter © 2007 Elsevier B.V. All rights reserved.
doi:10.1016/j.jpowsour.2007.11.106

newly formed oxygen-containing species are a strong oxidizing agent.

Many previous studies have employed noble metals and metal oxides as the oxygen electrode catalyst materials for the PEMWE or RPEMFC [2–21]. It is well known that platinum, the best catalyst for oxygen reduction, is not the best catalyst for oxygen evolution because of its high anodic overpotential (1.2 V at 1 A cm^{-2}) [2]. Oxides of noble metals such as iridium oxide (IrO_2) and ruthenium oxide (RuO_2) have been suggested for the OER. Compared with metallic platinum, IrO_2 offers a high activity (lower anodic overpotential at high current density, 100 mV at 1 A cm^{-2}), a better long-term stability (at least 2 years) and less efficiency loss due to corrosion or poisoning [2–7]. RuO_2 is somewhat more active for the OER compared to IrO_2. However, its thermal instability makes RuO_2 unsuitable for long-term oxygen evolution [2,4]. Calcination at 350 °C improves the thermal stability of RuO_2 at higher current density (1.1 A cm^{-2}) [8]. In addition, RuO_2 and IrO_2 are often mixed with inert components such as Ta_2O_5 or SnO_2 to stabilize their structures [9–16]. Adding Ta_2O_5 and SnO_2 to IrO_2 improves the anodic stability and catalytic activity [12–16]. Ir, IrO_2 or IrO_2–RuO_2, etc. catalysts have also been used in the bifunctional electrodes of RPEMFC for improving the oxygen evolution performance [17–21]. Yet the loadings of noble metals on these electrodes are quite high (1.5–2.0 mg cm^{-2}) [11].

The importance of the catalyst support for oxygen electrodes has been well accepted. Typically, the support should provide good electronic conductivity and a porous structure with reasonably high surface area. Carbon, which has good electronic conductivity and a suitable porous structure, has generally been used as the catalyst support in FC [22–26]. The use of carbon support materials permits a large reduction of the noble metal loadings on electrodes. However, the electrochemical oxidation of carbon during the oxygen evolution process in the PEMWE or RPEMFC sets a practical limit on the lifetime of the supported catalyst. Conductive supports including titanium [27], titanium oxides [28–33], boron carbide [34], and some perovskite compounds [35,36] have been reported as alterative support materials for use in the oxygen electrodes of FC. Other supports such as SiO_2 [37–39], Nb_2O_5 [40], onion-like fullerenes (OLFs) [41], CeO_2 and ZrO_2 [33,42–45], etc. were also studied. It is found that catalyst supports indeed increase the dispersion of metal catalysts as well as surface exposure and there is a significant electronic interaction between the catalysts and the support material, which leads to a substantial increase in catalyst utilization [28]. However, the supported catalysts used for the OER are less discussed in the literature.

Nano-materials have important applications in electrochemical catalysis because of their extremely high surface areas. The use of nano-metric components can lead to an improvement in the performance of many materials. Nano-sized titanium carbide (TiC) is chosen as the support material for this work because of its electrochemical and thermal oxidation stability and relatively high surface areas.

In the present study, we tried to develop a highly active supported catalyst for the OER in PEMWE. The Ir/TiC catalyst was prepared by chemical reduction and deposition with ultrasonic dispersion on nano-sized TiC support and characterized by physical and electrochemical means. Its electrochemical activity for the OER was investigated and compared with the unsupported Ir catalyst.

2. Experimental equipment and procedures

2.1. TiC support and characterization

The TiC support used was purchased from Fujian Sinocera Advanced Materials Co., LTD. The Brunauer–Emmet–Teller (BET) specific surface area of the TiC support was measured using a Micromeritics ASAP 2010 M + C. The sample was dried under vacuum at 60 °C for 15 h prior to analysis. A standard isotherm was obtained using liquid N_2 at 77 K. The XRD pattern was recorded by means of a Rigaku D/max2000 with an area detector using a Cu Kα radiation source (λ = 1.54056 Å) operating at 40 kV and 20 mA. The XRD sample was obtained by placing the test sample on a glass slide and then drying under vacuum overnight. The scanning angle (2θ) region between 20° and 80° was explored at a scan rate of 0.02° s^{-1}. The electrochemical performance of the TiC support material was studied by cyclic voltammograms (CVs), potentiostatic measurements and EIS, and the titanium (Ti) cations dissolved in the electrolyte solution were analyzed for examining stability of the TiC by inductively coupled plasma–atomic emission spectrometry (ICP) on an IRIS Advantage 1000.

2.2. Preparation of the Ir/TiC catalyst

The Ir/TiC catalyst was prepared by chemical reduction and deposition with ultrasonic dispersion. The TiC powders were dipped in de-ionized water containing the appropriate amount of isopropanol to form a suspended phase. The slurry was dispersed in an ultrasonic reactor for 10 min at room temperature. $(NH_2)_2IrCl_6$ (Alfa Aesar) was added to the above slurry in the calculated amount for the desired loading. The aqueous solution was subsequently heated to 80 °C and stirred under ultrasonic agitation. The reducing agent ($HCHO:NH_3:H_2O \approx 2:1:21$, weight ratio) was added to the mixture at 80 °C over a period of 40 min and the mixture was kept at 80 °C under ultrasonic agitation for an hour. After cooling to room temperature, the reduced and precipitated slurry was washed repeatedly with de-ionized water until the content of chlorine anion (Cl^-) in the filtrate dropped below 40 ppm. After drying at 80 °C for an hour, the filter cake was then set in a tube furnace and annealed at 500 °C for 30 min under flowing Argon before cooling down to room temperature. The Ir catalyst loading on the TiC support was 20 wt.%.

2.3. Ir/TiC characterization

The BET specific surface area and XRD pattern of the Ir/TiC were measured by the same methods as were used for the TiC support.

The morphological characteristics of the Ir/TiC were investigated by SEM using a FEI SIRION 200 operated at 5.00 KV. The chemical composition of the Ir/TiC was determined by EDX using an INCA OXFORD attached to the SEM. The particle size and size-distribution of the Ir/TiC catalyst were determined by TEM using a JEOL JEM-2010 microscope operated at 200 keV. The TEM sample was prepared by placing a drop of catalyst suspension in ethanol on a 3 mm copper grid, followed by drying at ambient conditions.

2.4. Working electrode preparation

Appropriate amounts of catalyst or support were ultrasonically suspended in a small quantity of a mixture of de-ionized water, isopropanol and the calculated quantity of Nafion solution (5 wt.% Nafion, Dupont) to prepare the catalyst or support ink. Then, 5 μl of ink was taken with a dram transfer instrument and deposited on a clean glassy carbon disk electrode (gcde) with a cross-sectional area of 0.07069 cm^2 (CHI104, CH Instrument co.) held in a Teflon cylinder. The electrode was dried under an infrared lamp at 40 °C for 10 min. A uniform catalyst or support layer was obtained as the working electrode. The loading of the support TiC, unsupported Ir and Ir as in Ir/TiC on the working electrode was about 0.02 mg.

2.5. Electrochemical measurements

A glass electrochemical system with a three-electrode configuration was used for the electrochemical experiments. A saturated calomel electrode (SCE) in saturated potassium chloride (KCl) solution, which was positioned as close to the working electrode as possible by means of a Luggin capillary, was used as the reference electrode. The counter electrode used was a 1 cm × 1 cm platinized Pt foil and the working electrode was the gcde containing support or catalyst. All potentials reported in this work were corrected with respect to the SCE.

In order to determine the catalytic activity of the Ir/TiC, unsupported Ir and support TiC for the OER, CV, potentiostatic and EIS experiments were carried out at room temperature (23 ± 2 °C). All the experiments were performed in 0.5 M H_2SO_4 solution prepared from high-purity sulfuric acid and de-ionized water. The potential range of the CVs was between −0.4 and 1.5 V with a scan rate of 50 mV s^{-1}. The potentiostatic data were obtained at a potential of 1.3 V. Data were collected using a Solartron Electrochemical Interface (model SI 1287) and the Corrware software.

EIS experiments were carried out at frequencies from 100 kHz to 0.1 Hz. The impedance spectra were registered with a logarithmic data collection scheme at 10 steps per decade with an amplitude of 10 mV at the desired potential. The impedance characterization was done by a Solartron Impedance/Gain-Phase Analyzer (model SI 1260) combined with a Solartron Electrochemical Interface (model SI 1287) and the Z-plot and Z-view software were used for data processing. The electrolyte solution and surfaces of the electrodes were de-aerated with nitrogen bubbling before and during the measurements.

Table 1
BET specific surface areas of the support and catalysts

Support and catalysts	BET specific surface areas (m^2 g^{-1})	Pore volume (cm^3 g^{-1})
TiC	14.41	0.0765
Ir	32.10	0.0647
Ir/TiC (20% Ir and 80% TiC, wt.)	14.62	0.1425

3. Results and discussion

3.1. BET analysis

The BET specific surface areas of the TiC support, Ir black (Johnson Matthey) and Ir/TiC catalyst prepared in this work are given in Table 1. The specific surface area of the TiC support is 14.41 m^2 g^{-1}, which is higher than those of Ebonex, phase-pure microcrystalline Ti_4O_7 and $Ti_{0.9}Nb_{0.1}O_2$ reported by Chen et al. [28]. The specific surface area of the Ir/TiC catalyst is higher than that of the TiC support. It can be seen that the pore volume of the supported Ir/TiC catalyst is about two times as high as that of the unsupported Ir with the same active composition, which indicates that the active component Ir of the Ir/TiC catalyst is predominantly dispersed on the outside surface of the TiC support and the TiC support changes the specific pore volume of the catalyst.

3.2. XRD analysis

The phase compositions of the TiC support, unsupported Ir and Ir/TiC catalyst were determined by XRD analysis. The XRD patterns are given in Fig. 1. The characteristic intense diffraction peaks of Ir (1 1 1), Ir (2 0 0) and Ir (2 2 0) can be found for the Ir and Ir/TiC samples. It is shown that the Ir supported on TiC forms a face-centered cubic (fcc) structure and has major peaks at around $2\theta = 40.8°$ (1 1 1), 47.4° (2 0 0) and 69.4° (2 2 0) using the TiC as an internal standard. It can be seen from Table 2 that the average crystal lattice parameter of the Ir deposited on

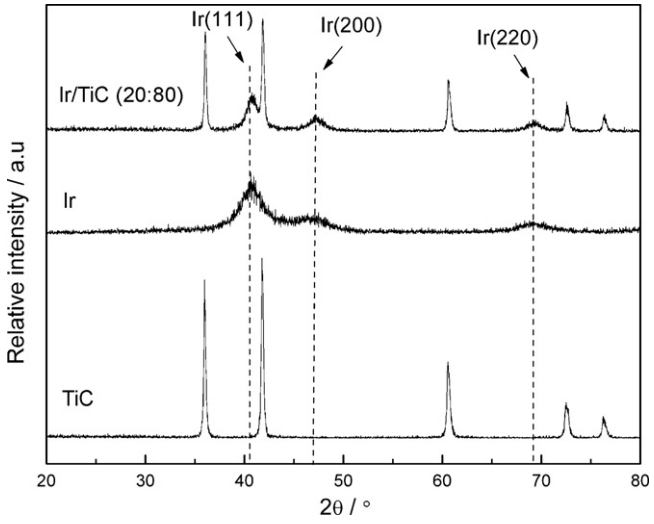

Fig. 1. XRD patterns of the TiC, Ir black and Ir/TiC.

Table 2
The lattice parameter of Ir on the Ir/TiC catalyst calculated by XRD patterns

h k l	2θ (°)		Crystal lattice parameter $\alpha_{fcc\ (Å)}$	
	Theoretic	Observed	Theoretic	Calculated
1 1 1	40.673	40.8		
2 0 0	47.318	47.4	3.839	3.8286
2 2 0	69.154	69.4		

the TiC is 3.8286 Å calculated by using the corresponding *h k l*, theoretical and observed values of 2θ. The calculated crystal lattice parameter is smaller than theoretical value. The difference in crystal lattice parameter of the Ir deposited on the TiC is probably attributed to the difference in crystallite form. At the same time, the evident broadening of the corresponding diffraction peaks of the Ir on the TiC reflects that the Ir crystal particles have high dispersion on the TiC support with much smaller sizes and crystallite form. Nano-sized crystallites will produce more crystal lattice defects, which usually are the highly active sites. The increase of crystal lattice defects improves the density of highly active sites. The small sizes of the Ir crystal particles on the TiC results in the high specific surface area of the Ir/TiC catalyst, thus the higher electrode surface area. The high electrode surface area means lower overpotential at the same current density for a high-performance oxygen electrode [46]. In other words, the Ir/TiC catalyst, which exhibits fine dispersion of the Ir particles on the TiC support, is a favorable candidate for an electrode material of improved catalytic activity.

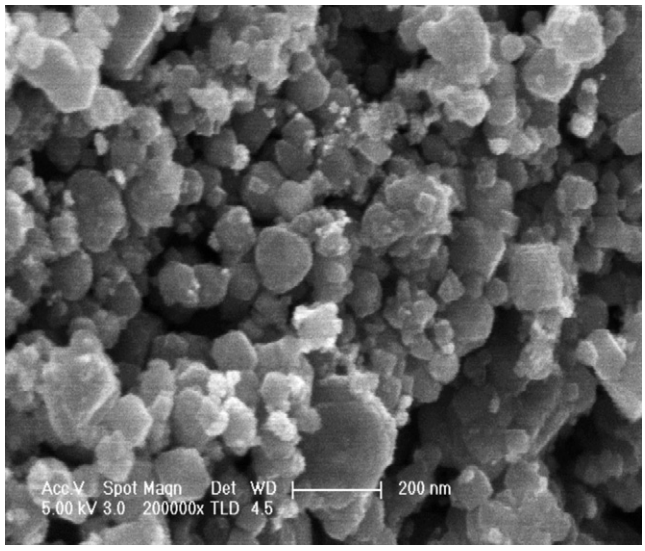

Fig. 2. SEM image of the Ir/TiC.

Table 3
EDX data of the Ir/TiC catalyst

Elements	Region 1		Region 2	
	Weight%	Atomic%	Weight%	Atomic%
C	35.55	72.18	21.89	54.87
Ti	51.38	26.16	69.73	43.82
Ir	13.07	1.66	8.38	1.31

3.3. SEM and TEM analysis

The SEM and TEM images of the Ir/TiC catalyst presented in Fig. 2, and Fig. 3a and b shows the Ir distribution on the TiC support. The formation and size of the particles are not well defined, possibly due to a certain agglomeration of the particles or sintering during sample preparation. The EDX spectra (Fig. 4a and b) and data (Table 3) were obtained by analyzing two different regions of the SEM image (Fig. 2) of the Ir/TiC catalyst. Ti, C and Ir are the major elements, confirming that the Ir particles are deposited on the surface of the TiC. The contents of the Ir in the Ir/TiC sample are, respectively, 8.38 and 13.07 wt.%, which are lower than the 20 wt.% theoretically calculated. The content difference detected in two different regions of the SEM can be ascribed to the fact that the detection depth of EDX is limited, and there is uneven dispersion in the preparation process.

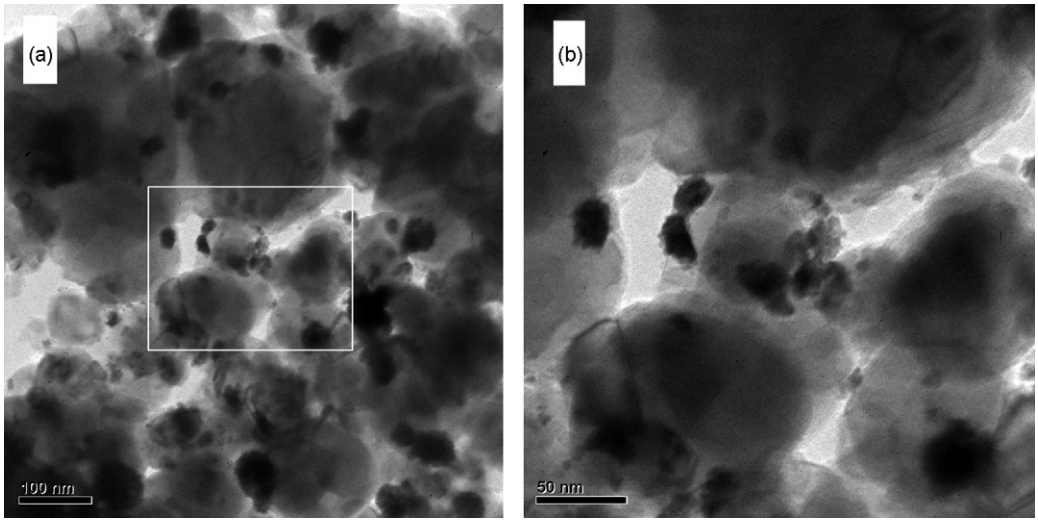

Fig. 3. TEM images of the Ir/TiC. Images (a) and (b) are respectively corresponding to the different resolution. Image (b) is magnification image of the region surrounded by white line in image (a).

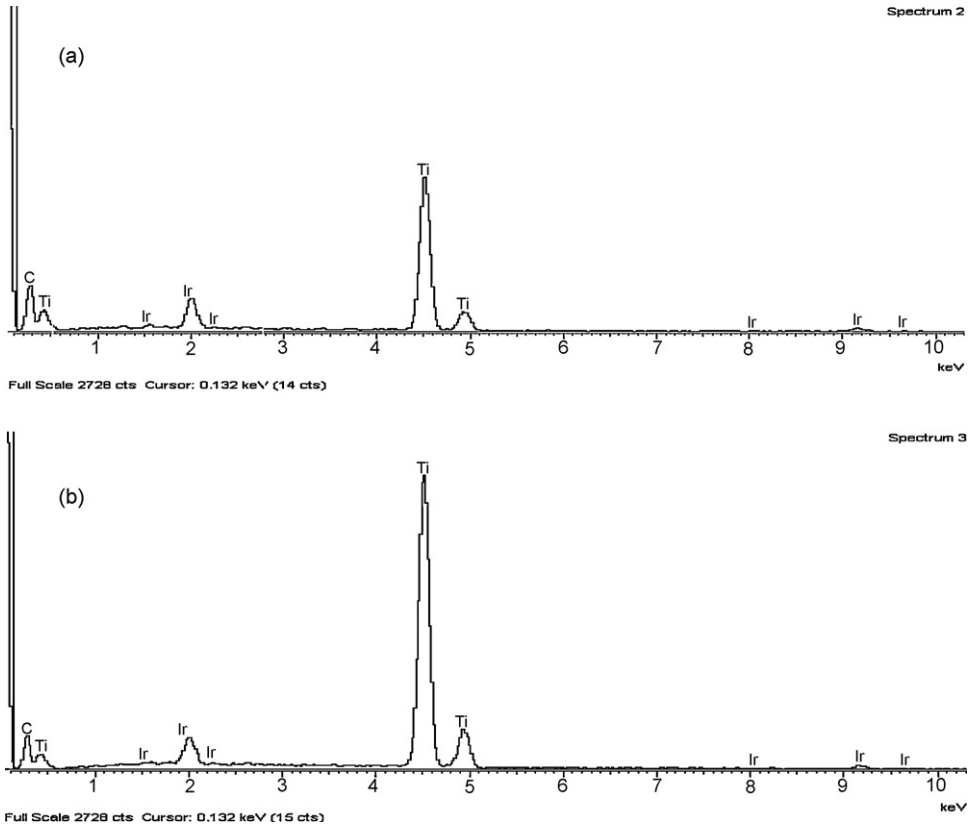

Fig. 4. EDX spectra of the Ir/TiC. Spectra (a) and (b) are respectively corresponding to the two different regions of SEM image on the Ir/TiC catalyst.

It is also possible that some nano-sized Ir particles went into the inside of pores among the TiC particles or were covered by them. The morphology of the TiC powders is spherical in shape and the particle sizes are about 50–150 nm as shown in Fig. 2. The particle sizes of the Ir deposited on the TiC are about 10–40 nm as represented in Fig. 3b. Since active components with smaller particle sizes give higher catalytic activity (Doyle et al. [47]), so the nano-particles Ir/TiC will increase the surface area and offer a high density of surface active sites to promote oxygen evolution.

3.4. CV analysis

CV measurements were done to evaluate the electrochemical activity of the TiC support, Ir black and Ir/TiC catalyst (20 wt.% Ir). The CV results are shown in Fig. 5a and b. The inserts in Fig. 5a and b are used to clearly show the starting potentials for the dynamical process of OER.

In the acid medium, the following reactions were generally proposed as the mechanism for OER on active electrodes. The

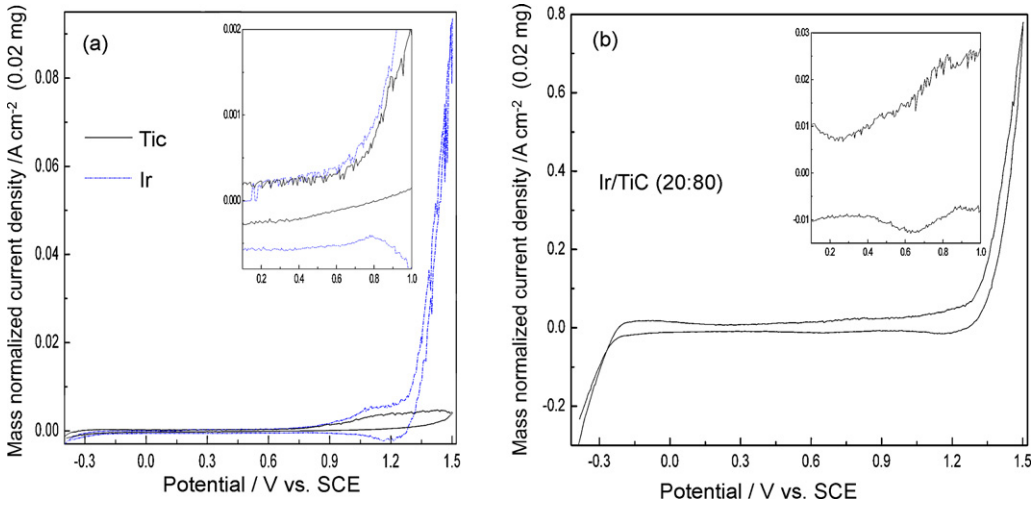

Fig. 5. Cyclic voltammogram curves of (a) the TiC and Ir black and (b) the Ir/TiC. The inserted patterns are respectively magnifications of the corresponding curves at the potential range of 0.1–1.0 V. Current densities are normalized to the 0.02 mg (for the TiC or Ir black) or the 0.02 mg Ir (for the prepared Ir/TiC).

active oxygen-containing species are catalyzed rapidly to form the oxygen molecule (see (1)–(4)) according to the mechanism of OER analyzed by Hu, Bockris, Damjanovic and Faria [48–51].

$$S + H_2O \rightarrow S\text{–}(H_2O)_{ads} \quad (1)$$

$$S\text{–}(H_2O)_{ads} \rightarrow S\text{–}OH_{ads} + H^+ + e^- \quad (2)$$

$$S\text{–}OH_{ads} \rightarrow S\text{–}O_{ads} + H^+ + e^- \quad (3)$$

$$S\text{–}O_{ads} + S\text{–}O_{ads} \rightarrow 2S + O_2 \quad (4)$$

Here, S stands for active sites on the surface of catalysts. $(H_2O)_{ads}$, OH_{ads} and O_{ads} represent adsorbed water molecules, adsorbed hydroxyl species and adsorbed oxygen atom, respectively.

It can be seen from Fig. 5a and b that the dynamical processes of the OERs for TiC, Ir black and Ir/TiC start at potentials about 0.6, 0.6 and 0.4 V with respect to the SCE, respectively. It suggests that the Ir deposited on the TiC has lower initial potential of the OER. The TiC support shows a slow oxygen evolution trend starting from a relatively higher potential of about 0.6 V. The TiC support exhibits a much weaker current density of oxygen evolution at 1.5 V in comparison with the Ir black and Ir/TiC catalysts. It proves that the TiC is an electrochemically inert material in the whole range of experimental potentials. It is obvious that the peak current density on the Ir/TiC, and thus the catalytic activity, is higher than that on the Ir black at the same experimental potential.

For comparison purposes, it is common to take the value of the kinetically controlled peak current density at a potential of 1.5 V. In the present experiments, it can be found that the peak current densities are 0.780 A cm^{-2} for the supported Ir/TiC and 0.089 A cm^{-2} for the Ir black, respectively. The catalytic activity on the Ir/TiC catalyst is about nine times that of the Ir black for the OER. All of these results indicate that the use of the TiC as support results in lower initial potential of the dynamical process for the OER and higher peak current density.

3.5. Potentiostatic analysis

Potentiostatic analysis is used to check the performance of these support and electrocatalyst materials as oxygen evolution electrocatalysts. Each of the electrodes was pretreated at 1.3 V for 120 s before data collection. The electric charge–time curves of the TiC, Ir black and Ir/TiC catalysts were recorded by maintaining the working electrodes at a potential of 1.3 V for 600 s and shown in Fig. 6. At the applied potential of 1.3 V, the Ir/TiC electrode exhibits the highest passage of electric charge compared to the TiC and Ir black electrodes. For example, after 600 s, the electric charge passed by the TiC, Ir black and Ir/TiC electrodes are about 0.2, 0.5 and 7.4 C cm^{-2} per 0.02 mg, respectively. The electric charge passed by the Ir/TiC electrode is about 15 times that of the Ir black electrode and 37 times that of the TiC electrode. It can be seen that the rate of increase in charge passed by the Ir/TiC electrode shows a slight decline with time, while that of the Ir black and TiC electrodes remains basically unchanged. This is probably due to the increasing obstruction formed by the tiny oxygen bubbles produced during oxygen evolution on the surface of the Ir/TiC. The remarkably different behaviors of charge passed by the TiC, Ir black and Ir/TiC electrodes indicate that the TiC is almost inert under these experimental conditions and the Ir/TiC displays the higher catalytic activity in comparison with the unsupported Ir.

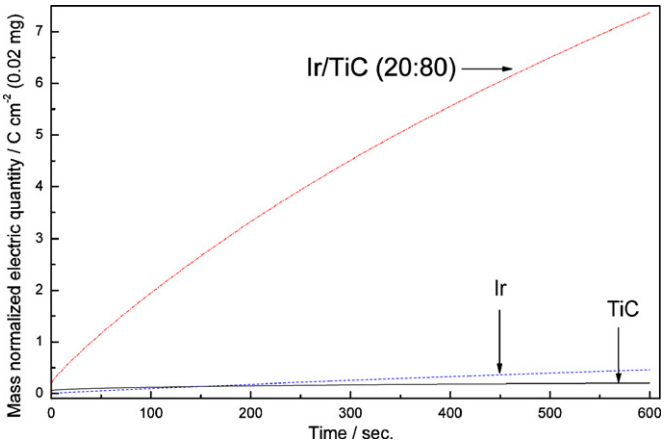

Fig. 6. Electric quantity–time curves of the TiC, Ir black and Ir/TiC. Electric quantities are normalized to the 0.02 mg (for the TiC or Ir black) or the 0.02 mg Ir (for the prepared Ir/TiC).

3.6. EIS analysis

EIS is a frequency domain method and a useful tool in analyzing the kinetics of electrode reactions. It provides much more information about the system studied than steady-state techniques, as different processes exhibit different relaxation times, which can be resolved in the frequency domain. The EIS technique has been used to investigate electrode reaction mechanisms [6,8,26,27,52–57].

Impedance plots of the TiC, Ir black and Ir/TiC electrodes at the potential of 0.8 V are recorded and shown in Fig. 7a and b. The frequency range was 100 kHz to 0.1 Hz. Fig. 7a shows the impedance plots of the TiC composed of an arc close to semicircle in the range of whole frequency. The impedance plots of the TiC are, respectively, in the shape of a straight line in the range of high and low frequencies, which show very high electrochemical polarization impedances and diffusion polarization impedances. The impedance plots of the Ir black and Ir/TiC are shown in Fig. 7b. The impedances of the Ir black are in the form of an arc close to semicircle in the range of high frequency and initial segment of an arc with big radius in the range of low frequency. The impedances of the Ir/TiC are consisted of two different arcs close to semicircle in the range of high and low frequencies, respectively. In the range of high frequency, the impedances on both imaginary (Z'') and real axes (Z') of the Ir/TiC are much lower than those of the Ir black. As shown in Fig. 7b and Fig. 8, when the simulating curves of semicircle arcs corresponding to the Ir black and Ir/TiC were extended to intersect with the real axes (Z'), the diameters of semicircle arcs are the corresponding electrochemical polarization impedances in the range of high frequency. The electrochemical polarization impedance of the Ir/TiC is about 100 Ω cm^2 per 0.02 mg catalyst and that of the Ir black is about 150 Ω cm^2. The electro-

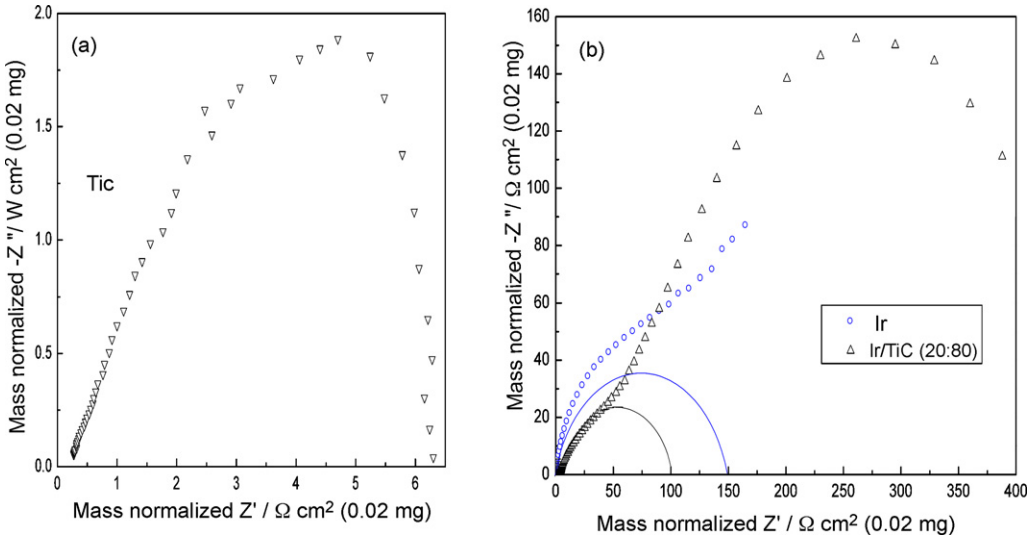

Fig. 7. EIS curves of (a) the TiC and (b) the Ir black and Ir/TiC. The Z' and Z'' are normalized to the 0.02 mg (for TiC or Ir black) or the 0.02 mg Ir (for the prepared Ir/TiC).

chemical polarization impedance of the Ir/TiC is about 50 Ω cm^2 lower than that of the Ir black. In addition, the impedances in the range of low frequency are the result of oxygen-containing species diffusion in catalytic layer. The impedances of the Ir black are close to a straight line with a phase angle of 45° in the range of low frequency. However, the impedances of the Ir/TiC form a semicircle, which proves that there exists obvious charge transfer. The lower diffusion polarization impedances of the Ir/TiC compared with those of the Ir black indicate that the Ir/TiC has higher catalytic activity for the OER at the potential of 0.8 V. These results confirm that the Ir/TiC sample presents much lower polarization resistance and significantly improves the catalytic activity for the OER in comparison with the Ir black. This is consistent with the results of the CV and potentiostatic measurements.

3.7. ICP analysis

ICP analysis was carried out to identify the stability of the support TiC in sulfuric acid electrolyte.

After the CV tests were conducted with the TiC electrode for five cycles with a scan rate of 100 mV s^{-1} and 60 cycles with a scan rate of 50 mV s^{-1}, the Ti contents in the sulfuric acid electrolytes were analyzed by ICP. After five cycles, the electrolyte contained 0.014 ppm Ti, which subsequently increased to 0.22 ppm after an additional 60 cycles. This demonstrates that the TiC is essentially not dissolved in the electrolytes and is chemically stable under the experimental conditions.

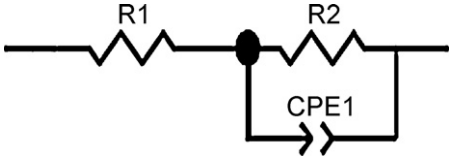

Fig. 8. Equivalent circuit (for the Ir and Ir/TiC) corresponding to the range of high frequency in Fig. 7. R_1: Ohmic resistance; R_2: high frequency semicircle arc resistance; CPE_1: high frequency semicircle arc constant phase element.

4. Conclusions

A systematic study was carried out on the performance of an Ir catalyst supported on TiC for oxygen evolution in a PEMWE. The possibility of using TiC as a catalyst support was demonstrated. The TiC support is a chemically and electrochemically inert material in the whole range of experimental potentials. The specific pore volume of the Ir/TiC catalyst is about two times as high as that of the corresponding unsupported Ir. The Ir particles deposited on the TiC support are about 10–40 nm in size and nearly uniformly disperse on the surface. The Ir/TiC results in a lower initial potential of the dynamical process for the OER. The peak current density at 1.5 V and charge passed after 600 s at 1.3 V on the Ir/TiC are respectively about nine times and 15 times those for the unsupported Ir catalyst. The electrochemical polarization impedance of the Ir/TiC is about 50 Ω cm^2 per 0.02 mg lower than 150 Ω cm^2 of the Ir black. The lower diffusion polarization impedances of the Ir/TiC compared with those of the Ir black form a semicircle, which proves that there exists obvious charge transfer and the Ir/TiC has higher catalytic activity at the potential of 0.8 V. All these prove that the catalytic activity on the Ir/TiC is much higher compared to the unsupported Ir for the OER.

Acknowledgements

This work is financially supported by the National Natural Science Foundation of China (Grant no. 20576071). We also thank Instrumental Analysis Center at Shanghai Jiao Tong University for their help on SEM, TEM and ICP tests. Professor Elton J. Cairns at chemical engineering department of UC Berkeley is acknowledged for his careful reading and suggestion in paper revising.

References

[1] A. Brassard, US Patent 6,579,638 (2003).
[2] F. Andolftto, R. Durand, A. Michas, P. Millet, P. Stevens, Int. J. Hydrogen Energy 19 (1994) 421–427.
[3] P. Millet, F. Andolftto, R. Durand, Int. J. Hydrogen Energy 21 (1996) 87–93.
[4] M. Yamaguchi, K. Ohisawa, T. Nakanori, Proceedings of the Intersociety Energy Conversion Engineering Conference, vols. 3–4, 1997, pp. 1958–1965.
[5] K. Ledjeff, F. Mahlendorf, V. Peinecke, A. Heinzel, Electrochim. Acta 40 (1995) 315–319.
[6] E. Rasten, G. Hagen, R. Tunold, Electrochim. Acta 48 (2003) 3945–3952.
[7] E. Slavcheva, I. Radev, S. Bliznakov, G. Topalov, P. Andreev, E. Budevski, Electrochim. Acta 52 (2007) 3889–3894.
[8] H.C. Ma, C.P. Liu, J.H. Liao, Y. Su, X.Z. Xue, W. Xing, J. Mol. Catal. A 247 (2006) 7–13.
[9] O. De Nora, G. Bianchi, A. Nidola, G. Trisoglio, US Patent 3,926,751 (1975).
[10] C.P. De Pauli, S. Trasatt, J. Electroanal. Chem. 396 (1995) 161–168.
[11] S.A. Grigoriev, V.I. Porembsky, V.N. Fateev, Int. J. Hydrogen Energy 31 (2006) 171–175.
[12] J.M. Hu, H.M. Meng, J.Q. Zhang, C.N. Cao, Corr. Sci. 44 (2002) 1655–1668.
[13] A. Marshall, B. Børresen, G. Hagenm, M. Tsypkin, R. Tunold, Electrochim. Acta 51 (2006) 3161–3167.
[14] A. Marshall, B. Børresen, G. Hagenm, M. Tsypkin, R. Tunold, Mater. Chem. Phys. 94 (2005) 226–232.
[15] K. Petrov, K.E. Xiao, E.R. Gonzalez, S. Srinivasan, A.J. Appleby, O.J. Murphy, Int. J. Hydrogen Energy 18 (1993) 907–913.
[16] S. Ardizzone, C.L. Bianchi, G. Cappelletti, M. Ionita, A. Minguzzi, S. Rondinini, A. Vertova, J. Electroanal. Chem. 589 (2006) 160–166.
[17] T. Ioroi, T. Okub, K. Yasuda, N. Kumagai, Y. Miyazaki, J. Power Sources 124 (2003) 385–389.
[18] G.Y. Chen, D.A. Delafuente, S. Sarangapani, T.E. Mallouk, Catal. Today 67 (2001) 341–355.
[19] L.L. Swette, A.B.L. Conti, S.A. McCatty, J. Power Sources 47 (1994) 343–351.
[20] T. Ioroi, N. Kitazawa, K. Yasuda, Y. Yamamoto, H. Takenaka, J. Appl. Electrochem. 31 (2001) 1179–1183.
[21] Y.J. Zhang, C. Wang, N.F. Wan, Z.Q. Mao, Int. J. Hydrogen Energy 32 (2007) 400–404.
[22] N. Jia, R.B. Martin, Z.G. Qi, M.C. Lefebvre, P.G. Pickup, Electrochim. Acta 46 (2001) 2863–2869.
[23] M.A. Fraga, E. Jordão, M.J. Mendes, M.M.A. Freitas, J.L. Faria, J.L. Figueiredo, J. Catal. 209 (2002) 355–364.
[24] S.R. de Miguel, J.I. Vilella, E.L. Jablonski, O.A. Scelza, C. Salinas-Martinez de Lecea, A. Linares-Solano, Appl. Catal. A 232 (2002) 237–246.
[25] M. Kim, J.N. Park, H. Kim, S. Song, W.H. Lee, J. Power Sources 163 (2006) 93–97.
[26] A.L. Ocampo, M. Miranda-Hernández, J. Morgado, J.A. Montoya, P.J. Sebastian, J. Power Sources 160 (2006) 915–924.
[27] Q.F. Yi, A.C. Chen, W. Huang, J.J. Zhang, X.P. Liu, G.R. Xu, Z.H. Zhou, Electrochem. Commun. 9 (2007) 1513–1518.
[28] G.Y. Chen, S.R. Bare, T.E. Mallouk, Electrochem. Soc. 149 (2002) A1092–A1099.
[29] V. Rashkova, S. Kitova, T. Vitanov, Electrochim. Acta 52 (2007) 3794–3803.
[30] Y. Sato, Y. Soma, T. Miyao, S. Naito, Appl. Catal. A 304 (2006) 78–85.
[31] J. Pettersson, B. Ramsey, D. Harrison, J. Power Sources 157 (2006) 28–34.
[32] Lj.M. Vračar, N.V. Krstajić, V.R. Radmilović, M.M. Jakšić, J. Electroanal. Chem. 587 (2006) 99–107.
[33] H. Iida, A. Igarashi, Appl. Catal. A 303 (2006) 192–198.
[34] W.T. Grubb, D.W. McKee, Nature 210 (1966) 192.
[35] A.C.C. Tseung, H.L. Bevan, J. Electroanal. Chem. 45 (1973) 429–438.
[36] M. Bursell, M. Pirjamali, Y. Kiros, Electrochim. Acta 47 (2002) 1651–1660.
[37] T. Miyao, Y. Watanabe, M. Teramoto, S. Naito, Catal. Commun. 6 (2005) 113–117.
[38] F. Locatelli, B. Didillon, D. Uzio, G. Niccolai, J.P. Candy, J.M. Basset, J. Catal. 193 (2000) 154–160.
[39] T. Tamai, M. Haneda, T. Fujitani, H. Hamada, Catal. Commun. 8 (2007) 885–888.
[40] K.V.R. Chary, C.P. Kumar, A. Murali, A. Tripathi, A. Clearfield, J. Mol. Catal. A 216 (2004) 139–146.
[41] B.S. Xua, X.W. Yang, X.M. Wang, J.J. Guo, X.G. Liu, J. Power Sources 162 (2006) 160–164.
[42] E. Guglielminotti, F. Boccuzzi, M. Manzoli, F. Pinna, M. Scarpa, J. Catal. 192 (2000) 149–157.
[43] P. Fornasiero, J. Kašpar, V. Sergo, M. Graziani, J. Catal. 182 (1999) 56–69.
[44] C. Bozo, N. Guilhaume, J.M. Herrmann, J. Catal. 203 (2001) 393–406.
[45] J. Mikulová, S. Rossignol, J. Barbier Jr., D. Mesnard, C. Kappenstein, D. Duprez, Appl. Catal. B 72 (2007) 1–10.
[46] J.W. Teng, L.H. Jin, L.C. Tang, Electrochemistry 4 (1997) 428–432.
[47] D.M. Doyle, G. Palumbo, K.T. Aust, A.M. EL-Sherik, U. Erb, Acta Metall. Mater. 43 (1995) 3027–3033.
[48] J.M. Hu, J.Q. Zhang, C.N. Cao, Int. J. Hydrogen Energy 29 (2004) 791–797.
[49] J.O'.M. Bockris, J. Chem. Phys. 24 (1956) 817.
[50] A. Damjanovic, A. Dey, J.O'.M. Bockris, Electrochim. Acta 11 (7) (1966) 791–814.
[51] L.A. De Faria, J.F.C. Boodts, S. Trasatti, J. Appl. Electrochem. 26 (11) (1996) 1195–1199.
[52] Z.B. Wang, G.P. Yin, Y.Y. Shao, B.Q. Yang, P.F. Shi, P.X. Feng, J. Power Sources 165 (2007) 9–15.
[53] G.Y. Chen, C.C. Waraksa, H. Cho, D.D. Macdonald, T.E. Mallouk, J. Electrochem. Soc. 150 (2003) E423–E428.
[54] X.Z. Yuan, J.C. Sun, H.J. Wang, J.J. Zhang, J. Power Sources 161 (2006) 929–937.
[55] A.A. Sagüés, J.T. Wolan, A. De Fex, T.J. Fawcett, Electrochim. Acta 51 (2006) 1656–1663.
[56] W. Mérida, D.A. Harrington, J.M. Le Canut, G. McLean, J. Power Sources 161 (2006) 264–274.
[57] E.B. Easton, P.G. Pickup, Electrochim. Acta 50 (2005) 2469–2474.